Phase coexistence and pinning of charge density waves by interfaces in chromium

A. Singer,[1,*] S. K. K. Patel,[1,2] V. Uhlíř,[2] R. Kukreja,[1,2] A. Ulvestad,[1,†] E. M. Dufresne,[3]
A. R. Sandy,[3] E. E. Fullerton,[2] and O. G. Shpyrko[1]
[1]*Department of Physics, University of California San Diego, La Jolla, California 92093, USA*
[2]*Center for Memory and Recording Research, University of California San Diego, La Jolla, California 92093, USA*
[3]*Advanced Photon Source, Argonne National Laboratory, Argonne, Illinois 60439, USA*
(Received 6 September 2016; revised manuscript received 22 October 2016; published 16 November 2016)

We study the temperature dependence of the charge density wave (CDW) in a chromium thin film using x-ray diffraction. We exploit the interference between the CDW satellite peaks and Laue oscillations to determine the amplitude, the phase, and the period of the CDW. We find discrete half-integer periods of CDW in the film and switching of the number of periods by one upon cooling/heating with a thermal hysteresis of 20 K. The transition between different CDW periods occurs over a temperature range of 30 K, slightly larger than the width of the thermal hysteresis. A comparison with simulations shows that the phase transition occurs as a variation of the volume fraction of two distinct phases with well-defined periodicities. The phase of the CDW is constant for all temperatures, and we attribute it to strong pinning of the CDW by the mismatch-induced strain at the film-substrate interface.

DOI: 10.1103/PhysRevB.94.174110

I. INTRODUCTION

Antiferromagnetic materials have been intensively studied in recent decades and gained increased interest with the advent of spintronics. These materials were initially implemented in giant magnetoresistive read heads to pin the reference layer through the exchange bias interaction [1,2]. In these applications, the functionality of the antiferromagnetic layer arises from the perturbation of a ferromagnetic layer. However, more recent research has focused on directly using the antiferromagnetic order in spintronic devices [3]. The careful engineering of the antiferromagnetic domains found applications in data storage and data transport [4], and imaging techniques with sufficient spatial resolution are required to develop new spintronic materials and devices systematically. X-ray diffraction is superb in studying the structure of crystalline materials and its distortions in the presence of antiferromagnetism. The brightness of synchrotron radiation is particularly useful for the understanding of these phenomena in thin films.

Chromium (Cr) is the archetypal antiferromagnetic material. Below the Néel temperature (311 K in bulk [5] and around 290 K in thin films [6–9]), Cr is antiferromagnetic and exhibits an incommensurate spin density wave (SDW) and a charge density wave (CDW). The CDW is a second harmonic of the SDW, is coupled to the SDW, and has a period between 3 and 4 nm depending on the temperature [5,7]. In thin-films grown along the [001] direction, the SDW/CDW usually has the wave vector pointing normal to the film surface with spins lying in the film plane [7,10]. The SDW/CDW period is quantized due to confined geometry and follows a thermal hysteresis [8,11–13]. Pinning of the SDW and CDW in Cr by impurities was studied theoretically [14,15] and experimentally [16]. Weak pinning was expected for the SDW and strong pinning for the CDW [14]. In confined geometries, further experimental studies revealed pinning of the SDW by the spin structure at interfaces; antinodes of the SDW were observed in Cr/CrMn multilayers [8], and nodes were found in Cr/Fe systems due to interface roughness [6,7]. In thin Cr films grown on MgO, half-integer periods of the CDW were found [9,13].

In Cr, the CDW can be readily detected in x-ray diffraction experiments: The reciprocal space contains not only Bragg peaks but also satellites due to the periodic lattice distortion associated with the CDW [see Fig. 1(a)]. In relatively thick samples, only the intensity and position of the satellites can be measured to determine the amplitude and period of the CDW, while the phase of the CDW is lost [7]. For thin films (∼30 nm), however, interference between the Laue oscillations and satellites allows an efficient determination of the CDW phase [13]. Here we use this interference to study the amplitude, period, and phase of the CDW in a Cr thin film as a function of temperature upon cooling and heating in the range between 10 K and 300 K.

II. EXPERIMENTAL DETAILS

A thin Cr film was deposited onto single-crystal MgO (001) substrate using magnetron sputtering at a substrate holder temperature of 500 °C and then annealed for 1 h at 800 °C. The growth process was optimized to yield both a smooth surface and good crystal quality of the sample [17]. We performed in-house x-ray diffraction characterization of the sample at room temperature [see Fig. 1(b)]. The x-ray reflectivity curve revealed a film thickness of about 30 nm. It further showed the presence of the oxide layer (∼2 nm thick). An azimuthal scan around the (011) peak confirmed the epitaxial growth of the Cr film on MgO [see left inset in Fig. 1(b)]. A Gaussian fit to the θ-2θ scan of the (011) peak [see right inset in Fig. 1(b)] revealed a mosaic spread in the sample plane with a typical domain size of about 25 nm. This inhomogeneity likely appears due to a small mismatch between the in-plane MgO and Cr lattices. The interatomic spacing of the (011) planes of MgO

*Email address: ansinger@ucsd.edu
†Present address: Materials Science Division, Argonne National Laboratory, Lemont, Illinois 60439, USA.

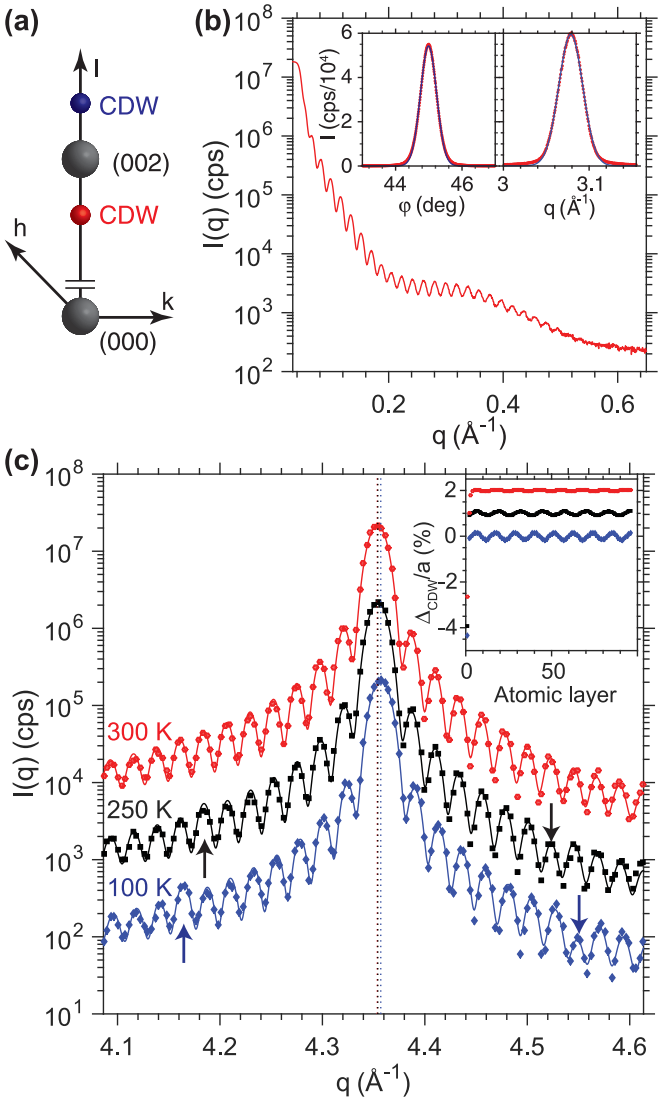

FIG. 1. (a) Sketch of the reciprocal space around the (002)-diffraction peak of Cr in the presence of a CDW. (b) X-ray reflectivity measurement of the Cr thin film with Cu K-α radiation. (Left inset) The φ rotation scan (right inset) and θ-2θ scan around the (011) peak (out of plane). In both insets, red dots show the data, and blue solid lines show Gaussian fits used to determine the peak widths. (c) A θ-2θ scan around the (002) peak recorded with synchrotron radiation at room temperature (red hexagons), 250 K (black squares), and 100 K (blue diamonds). Solid lines show theoretical fits to the data, and vertical dashed lines show the center of the Bragg peak. Inset: The corresponding lattice distortion or displacement; the curves are shifted vertically for better visibility.

is 3.4% larger than the interatomic spacing of (001) planes of Cr, presumably inducing defects in Cr every 30 unit cells on average ($\sim$10 nm).

Temperature dependent x-ray diffraction studies were performed at beamline 8 ID-E of the Advanced Photon Source at the Argonne National Laboratory. A photon energy of 7.35 keV was selected by a silicon (111) double crystal monochromator. The sample was mounted inside a He flow cryostat [18], x rays were scattered vertically, and the diffracted radiation was recorded by a scintillator detector with a vertical slit (1 mrad in angular size) placed in front of the detector to increase angular resolution. Repeated θ-2θ scans around the out of plane (002) Bragg peak were collected for different temperatures ranging from 10 K to 300 K, while the film was continuously cooled or heated with rates between 2 K/min and 4 K/min.

III. RESULTS AND DISCUSSION

Shown in Fig. 1(c) is a scan recorded at a film temperature of 300 K. The high visibility of the Laue fringes due to a finite sample thickness demonstrates excellent crystal quality and uniform thickness over large sample areas (beam size of several hundreds of microns). Upon cooling below 300 K, the Bragg peak not only shifts to higher angles due to contraction of the lattice, but it also shows additional features. In particular, satellite peaks formed due to the presence of a CDW. The CDW does not lead to an increase in the diffracted intensity at both satellite positions [5,7,19]. Instead, the intensity is enhanced for the low-q and suppressed for the high-q peak due to constructive and destructive interference [13,17]. Noticeably, at 250 K the interference occurs on fringe number 7, while at 100 K the interference occurs on fringe 8 [see Fig. 1(c)], which indicates that the CDW periodicity shifts to a smaller period with temperature.

To get quantitative information from the x-ray data, we modeled it with the following expression:

$$I(q) = |F_{\mathrm{FILM}}(q) + F_{\mathrm{SUB}}(q)|^2, \tag{1}$$

where F_{FILM} and F_{SUB} are the fields scattered by the Cr film and the MgO substrate, respectively, and q is the momentum transfer along the [001] direction in the reciprocal space. The field scattered by the Cr film was calculated as a one-dimensional (1D) numeric summation over the atomic planes normal to q [20] $F_{\mathrm{FILM}} = f_{\mathrm{Cr}} \sum_{j=0}^{N-1} \exp(-iqz_j)$ positioned at

$$z_j = z_{0,j} + \Delta_{\mathrm{ST},j} + \Delta_{\mathrm{CDW},j}, \tag{2}$$

where N is the number of atomic layers, f_{Cr} is the scattering power per unit area of an atomic plane of Cr, $z_{0,j} = a_0 \cdot j$ is the undistorted position of the jth plane, a_0 is the average lattice parameter, and $\Delta_{\mathrm{ST},j} = a_1 \cdot \exp(-j/b)$ is the displacement at the substrate interface, which was modeled to relax exponentially with amplitude a_1 and relaxation distance b [21]. The periodic lattice distortion due to the CDW is described by the last term in Eq. (2), $\Delta_{\mathrm{CDW},j} = a_2 \cdot \cos(z_{0,j} \cdot Q + a_4)$, where a_2 is the amplitude, $Q = 2\pi \cdot a_3/[a_0(N-1)]$, a_3 is the number of periods of the CDW in the film, and a_4 is the phase of the CDW relative to the substrate interface. The field scattered by the substrate is given by $F_{\mathrm{SUB}} = f_{\mathrm{MgO}} \frac{1}{1-\exp(iqd_{\mathrm{MgO}})}$, where d_{MgO} is the MgO (002) lattice spacing and f_{MgO} is the scattering power per unit area of an atomic plane of MgO [22]. The finite experimental resolution was taken into account by summation of intensities from Eq. (1) with slightly different momentum transfers $q' = q(1+\varepsilon)$, weighted by a Gaussian function $\exp(-\varepsilon^2/[2 * dE^2])$, with ε having 30 points between $\pm 3dE$. The surface roughness σ was included by multiplying the scattered intensity by $\exp(-(q-q_{002})^2\sigma^2)$, where $q_{002} = 4\pi/a_0$ is the position of the Bragg peak [23].

The following fitting procedure was employed. First, the number of atomic layers N of Cr was calculated from the fringe spacing. Second, the strain relaxation parameter b,

surface roughness σ, and bandwidth dE were determined from the data at 300 K. Finally, five fit parameters were found at different film temperatures while fixing N, b, σ, and dE: the average lattice constant a_0, displacement of the Cr layer at the substrate interface a_1, amplitude a_2, number of periods a_3, and phase a_4 of CDW. The fixed parameters were found to be $N = 96$, $b = 0.64$, $\sigma = 3.2\,\text{Å}^{-1}$, and $dE = 7.4 \cdot 10^{-4}$. The peak is asymmetric, the low-q tail having about twice higher intensity than the high-q tail. We attribute this asymmetry to strain at the film-substrate interface, and the strain term $\Delta_{ST,j}$ in Eq. (2) is considered to be essential to reproduce the asymmetry of the x-ray data. The maximum displacement field obtained from the fit at 300 K is about 4% of the Cr unit cell size. The exceptionally large strain presumably occurs due to the large difference between the (001) lattice spacing of MgO (4.1 Å) and Cr (2.88 Å).

Typical fits to the data are shown in Fig. 1(c), in excellent agreement with the experiment over three orders of magnitude in intensity, and correctly reproduce the data at the positions of the CDW satellites. The displacement determined from the fit [see inset of Fig. 1(c)] shows both negative displacement at the interface and periodic modulations. The data at 100 K is consistent with a CDW having 8.5 periods in the film, while at 250 K, 7.5 periods are observed with reduced CDW amplitude. The CDW amplitude is negligible at 300 K. Presented in Fig. 2 are the determined fit parameters from the x-ray data recorded upon cooling (blue symbols) and heating (red symbols). The average lattice constant is in agreement with the thermal expansion coefficient of Cr reported in the literature [13,24] [see Fig. 2(a)]. It is also identical for both cooling and heating, demonstrating that although we measured the data while the sample was continuously cooled/heated, the temperature transport from the cryostat to the sample can be considered rapid compared with the measurement time and the cooling/heating rate. The displacement of the first layer is constant around 4% to the precision of the measurement and is not shown here. Figure 2(b) displays the amplitude of the CDW, which agrees well with the description using the Bardeen-Cooper-Schrieffer (BCS) theory [25,26] everywhere, except for the transition region (gray shaded area), where the used fit with only one CDW periodicity underestimates the CDW contribution.

The period of the CDW and its phase are presented in Figs. 2(c) and 2(d). As already anticipated from the inspection of the x-ray data, we observe two distinct temperature regions with $N_P = 7.5$ periods and $N_P = 8.5$ periods, suggesting strong pinning at the film boundaries. The number of CDW nodes displays hysteretic behavior, as expected from previous measurements in confined geometries [8,9,12,13]. The phase is constant to experimental accuracy and is slightly larger than π, indicating that the antinodes of the CDW are not exactly at the MgO interface and the surface. The constant phase indicates identical pinning conditions for different temperatures and different periodicities of the CDW. For all temperatures, our data is consistent with negative displacement and tensile strain due to the CDW at the substrate interface.

To get further insights into the transition between the phases of different CDW periodicities, we performed an additional measurement. We cooled the film at a similar rate (2 K/min) but now only recorded scans around the satellite peaks (3 fringes)

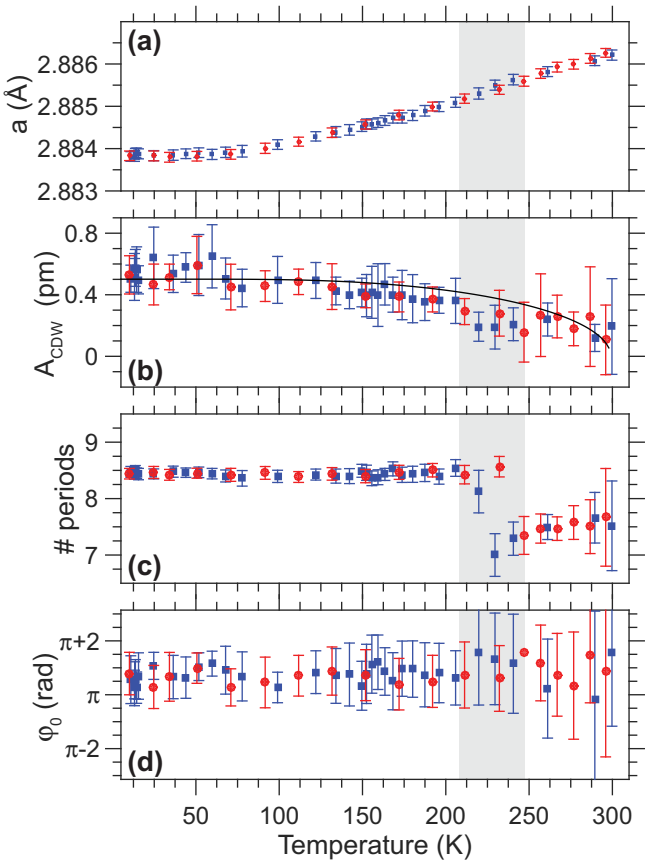

FIG. 2. Fitting results of the data for different temperatures. The average lattice parameter (a), amplitude (b), number of periods (c), and phase (d) of the CDW. The black line in (b) shows a calculation of the CDW amplitude within the BCS theory based on the maximum observed CDW amplitude and a Neel temperature of 290 K. Uncertainties show 95% confidence intervals, and the error metric $\chi^2 = \Sigma[\log_{10}(I_{th}) - \log_{10}(I_{exp})]^2/N$, where summation over the fitted points N was used for fitting. The gray shaded area represents the transition region between fringe 7 and fringe 8.

on both sides of the Bragg peak [see Figs. 3(a) and 3(b)]. As expected, upon cooling a slight shift of the fringes to higher q is observed, while fringe 7 at high temperatures and fringe 8 at low temperatures show the signature of the CDW. The limited q-range made fitting the data to Eq. (1) impossible. Instead, the intensities, $I_7(T)$, of the 7th and, $I_8(T)$, of the 8th fringes were found by approximating the five central data points of the respective fringe with a Gaussian [see Figs. 3(c) and 3(d)]. We describe the data at low q first (left column in Fig. 3). Upon cooling, we observe an approximately linear increase of $I_7(T)$, which shows that the CDW forms with $N_P = 7.5$ periods at the Néel transition and its amplitude grows with subsequent cooling. Below 240 K, $I_7(T)$ begins to drop quickly, while $I_8(T)$ rises as the temperature decreases. At 210 K through cooling, the temperature dependences of the intensities decrease abruptly, with $I_8(T)$ greater than $I_7(T)$. The high-q data shows similar behavior for $I_7(T)$ and $I_8(T)$; however, the slopes of the curves are reversed due to destructive interference, as compared with constructive interference at low-q. We repeated the measurement with a cooling rate of

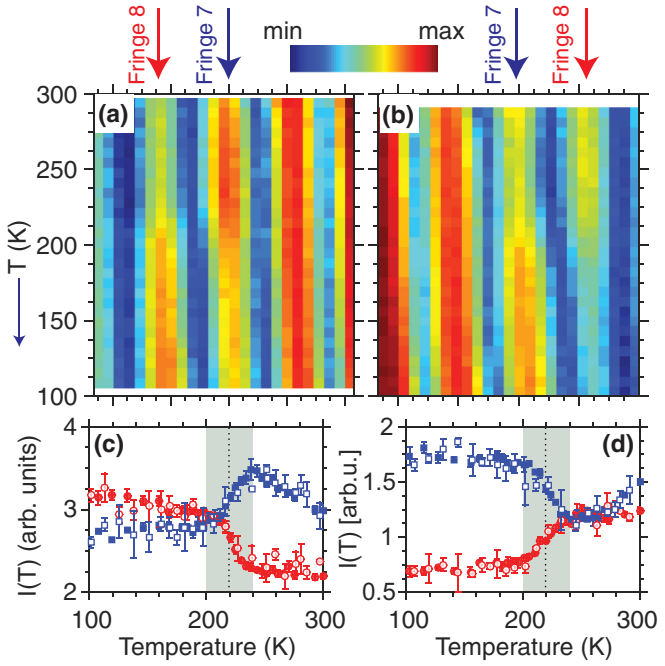

FIG. 3. X-ray diffraction intensity around the CDW peak upon cooling. Low-q (a) and high-q (b) with respect to the Bragg peak are shown. Fringes as counted from the Bragg peak are indicated [see Fig. 1(c)]. The intensities are shown on logarithmic scale. (c), (d) The intensity of fringe 7 (blue squares) and 8 (red circles) for low-q (c) and high-q (d). Filled (open) symbols show data collected with a cooling rate of 2 K/min (4 K/min). The gray shaded area represents the transition region between fringe 7 and fringe 8 and is approximately 30 K wide.

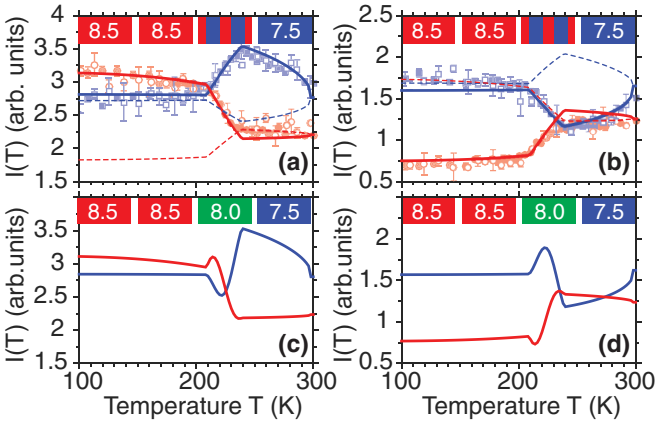

FIG. 4. Simulated diffraction patterns assuming abrupt (a), (b) and continuous (c), (d) phase transition between CDW phases with 7.5 and 8.5 periods. Calculations with a phase offset of $a_4 = 3.8$ rad (solid lines), and $3.8 + \pi/2$ rad (dashed lines) are shown. The data from Figs. 3(c) and 3(d) are shown by shaded symbols for comparison. Blue (red) lines show intensity of fringe 7 (8). Simulations at low-q (a), (c) and high-q (b), (d) are shown. The insets show schematically the composition of the phases.

4 K/min and found that it agrees well with the data collected at 2 K/min, demonstrating that the phase transition is not limited by the cooling rate in our experiment.

To get a deeper insight into the phase coexistence during the transition between CDW with different periods, we made the following model calculations (see Fig. 4). First, we simulated two distinct phases containing different numbers of periods $N_P = 7.5$ and $N_P = 8.5$ with a volume fraction of α and (1-α), respectively. We used $\alpha = 0$ for a temperature range between 100 and 210 K, $\alpha = 1$ from 240 to 300 K, and linearly interpolated α in the transition region. The temperature dependent amplitude of the CDW was determined in the framework of the BCS theory. The intensities $I_7(T)$ and $I_8(T)$ calculated using Eq. (1) are shown in Figs. 3(a) and 3(b) for different phases of the CDW. A comparison between the data and simulation [see solid lines for simulation and shaded symbols for the data in Figs. 4(a) and 4(b)] shows exemplary agreement, demonstrating that this simple model captures the essence of the physical processes involved in the phase transition. The best agreement is observed for a phase of $a_4 = \pi + 0.7$ and $a_1 = 0.025$, comparable to the values determined in the fits to the data [see Fig. 2(d)]. The sensitivity of the presented method to the phase of the CDW is demonstrated by another calculation with the phase $a_4 = \pi + 0.7 + \pi/2$ [see dashed line in Figs. 4(a) and 4(b)], which clearly disagrees with the data. A similar calculation assuming a continuous phase transition, where the periodicity changes continuously from $N_P = 7.5$ to $N_P = 8.5$ via $N_P = 7.5 \cdot \alpha + 8.5 \cdot (1 - \alpha)$, is also shown in Figs. 4(c) and 4(d). This calculation does not reproduce the experimental observation, rendering this interpretation incomplete.

IV. CONCLUSION

In conclusion, we have used x-ray diffraction to study pinning of the CDWs by interfaces in Cr as a function of temperature. The interference between the CDW peaks and Laue fringes allows us to determine not only the amplitude and the period of the CDW but also its phase on the interfaces. This phase provides insight into to the pinning of the CDW by the interfaces. Above the Néel transition, the data indicates tensile strain at the substrate interface (negative displacement as compared with the strain-free lattice). Below the Néel transition the CDW also has a negative displacement at the substrate interface, which suggests that the tensile strain at the interface pins the CDW. The temperature scans show that the CDW has a half-integer number of periods in the film at all temperatures. During cooling, the number of periods jumps from 7.5 above 240 K to 8.5 below 210 K. Upon heating, the transition occurs at higher temperatures, revealing a thermal hysteresis. Model simulations confirm a first order phase transition with a transition region of 30 K, coexistence of distinct phases containing either 8.5 or 7.5 periods, and identical pinning conditions at the film interfaces for both phases. This paper opens up ways to explore the phase coexistence of CDW and SDW in thin films. We anticipate this technique to be applicable to study other phenomena; for example, the phase of phonons in confined geometries. The apparent pinning of the CDW by interface strain promises advanced control of the spatial distribution of the structural order parameter in other correlated electron systems.

ACKNOWLEDGMENTS

The work at the University of California San Diego was supported by U.S. Department of Energy, Office of Science, Office of Basic Energy Sciences, under Contracts No. DE-SC0001805 (x-ray scattering, A.S., R.K., A.U., and O.G.S.) and No. DE-SC0003678 (thin films synthesis and characterization, S.K.K.P., R.K., V.U., and E.E.F.). R.K. acknowledges support by UC-MRPI Grant No. MR-15-328528. This research used resources of the Advanced Photon Source, a U.S. DOE Office of Science User Facility operated for the DOE Office of Science by Argonne National Laboratory under Contract No. DE-AC02-06CH11357.

[1] J. Nogués and I. K. Schuller, J. Magn. Magn. Mater. **192**, 203 (1999).
[2] I. R. McFadyen, E. E. Fullerton, and M. J. Carey, MRS Bull. **31**, 379 (2006).
[3] T. Jungwirth, X. Marti, P. Wadley, and J. Wunderlich, Nat. Nanotechnol. **11**, 231 (2016).
[4] S. A. Wolf, D. D. Awschalom, R. A. Buhrman, J. M. Daughton, S. von Molnár, M. L. Roukes, A. Y. Chtchelkanova, and D. M. Treger, Science **294**, 1488 (2001).
[5] E. Fawcett, Rev. Mod. Phys. **60**, 209 (1988).
[6] E. E. Fullerton, S. D. Bader, and J. L. Robertson, Phys. Rev. Lett. **77**, 1382 (1996).
[7] H. Zabel, J. Phys. Condens. Matter **11**, 9303 (1999).
[8] E. E. Fullerton, J. L. Robertson, A. R. E. Prinsloo, H. L. Alberts, and S. D. Bader, Phys. Rev. Lett. **91**, 237201 (2003).
[9] Y.-A. Soh and R. K. Kummamuru, Philos. Trans. R. Soc. A Math. Phys. Eng. Sci. **369**, 3646 (2011).
[10] J. M. Logan, H. C. Kim, D. Rosenmann, Z. Cai, R. Divan, O. G. Shpyrko, and E. D. Isaacs, Appl. Phys. Lett. **100**, 192405 (2012).
[11] R. Jaramillo, T. F. Rosenbaum, E. D. Isaacs, O. G. Shpyrko, P. G. Evans, G. Aeppli, and Z. Cai, Phys. Rev. Lett. **98**, 117206 (2007).
[12] R. K. Kummamuru and Y.-A. Soh, Nature **452**, 859 (2008).
[13] A. Singer, M. J. Marsh, S. H. Dietze, V. Uhlíř, Y. Li, D. A. Walko, E. M. Dufresne, G. Srajer, M. P. Cosgriff, P. G. Evans, E. E. Fullerton, and O. G. Shpyrko, Phys. Rev. B **91**, 115134 (2015).
[14] P. A. Lee and T. M. Rice, Phys. Rev. B **19**, 3970 (1979).
[15] P. B. Littlewood and T. M. Rice, Phys. Rev. Lett. **48**, 44 (1982).
[16] G. Teisseron, J. Berthier, P. Peretto, C. Benski, M. Robin, and S. Choulet, J. Magn. Magn. Mater. **8**, 157 (1978).
[17] A. Singer, S. K. K. Patel, R. Kukreja, V. Uhlíř, J. Wingert, S. Festersen, D. Zhu, J. M. Glownia, H. T. Lemke, S. Nelson, M. Kozina, K. Rossnagel, M. Bauer, B. M. Murphy, O. M. Magnussen, E. E. Fullerton, and O. G. Shpyrko, Phys. Rev. Lett. **117**, 056401 (2016).
[18] O. G. Shpyrko, E. D. Isaacs, J. M. Logan, Y. J. Feng, G. Aeppli, R. Jaramillo, H. C. Kim, T. F. Rosenbaum, P. Zschack, M. Sprung, S. Narayanan, and A. R. Sandy, Nature **447**, 68 (2007).
[19] P. Sonntag, P. Bödeker, T. Thurston, and H. Zabel, Phys. Rev. B **52**, 7363 (1995).
[20] B. E. Warren, *X-Ray Diffraction* (Courier Dover Publications, New York, 1969).
[21] E. E. Fullerton, I. K. Schuller, H. Vanderstraeten, and Y. Bruynseraede, Phys. Rev. B **45**, 9292 (1992).
[22] E. E. Fullerton, D. Stoeffler, K. Ounadjela, B. Heinrich, Z. Celinski, and J. A. C. Bland, Phys. Rev. B **51**, 6364 (1995).
[23] S. K. Sinha, E. B. Sirota, S. Garoff, and H. B. Stanley, Phys. Rev. B **38**, 2297 (1988).
[24] G. K. White, R. B. Roberts, and E. Fawcett, J. Phys. F Met. Phys. **16**, 449 (1986).
[25] J. Bardeen, L. N. Cooper, and J. R. Schrieffer, Phys. Rev. **108**, 1175 (1957).
[26] A. W. Overhauser, Phys. Rev. **128**, 1437 (1962).